

# Generation of realistic input parameters for simulation of atmospheric point-spread functions with psf-weather-station

CLAIRE-ALICE C. HÉBERT <sup>1,2</sup>, MYA DO,<sup>3</sup> JOSHUA E. MEYERS<sup>4</sup> AND PATRICIA R. BURCHAT<sup>1,5</sup>

THE DARK ENERGY SCIENCE COLLABORATION

<sup>1</sup>*Kavli Institute for Particle Astrophysics and Cosmology, ....*

<sup>2</sup>*Department of Applied Physics, Stanford University, ...*

<sup>3</sup>*Department of Physics, Cal-State University Pomona, ...*

<sup>4</sup>*Lawrence Livermore National Lab,...*

<sup>5</sup>*Department of Physics, Stanford University, ...*

## ABSTRACT

250 word limit for the abstract.

### 1. INTRODUCTION

Big surveys and big telescopes, more precise science, more and more important to have robust algorithms to process data and produce accurate results. Also always important to forecast how proposed instruments or measurements will perform. Both these things necessitate high-fidelity simulations of the telescope and its environment. One part of this is the contribution of the atmosphere to the point-spread function (PSF), of huge importance to adaptive optics, and, more recently, to precision cosmology/cosmic shear analyses, since atmospheric PSFs have significant spatial variation across a field of view (Jarvis et al. 2016; Heymans et al. 2012).

A focus on high-fidelity atmospheric PSF simulations is not new in the world of precision cosmology analyses; in the preparation for the Vera C Rubin Observatory, many studies have used the same thin-screen, frozen-flow simulation scheme that we use in this paper (Jee & Tyson 2011; Chang et al. 2012; Peterson et al. 2015; ?). Focus on DC2 and Peterson et al. (2015): both studies have chosen a different parameter initialization for the environmental conditions at the telescope of interest. DC2 paper uses random perturbations from the OTP of Ellerbroek (2002), and uniform wind information. Peterson et al. (2015) includes some improvements by drawing their wind and turbulence values from fits to historical data (NOAA and Tokovinin, respectively). This second method, while capturing realistic one-dimensional distributions for each parameter over time, does not account for altitude-dependent correlations of a single parameter at a given time, nor the relationship between wind and turbulence. **In addition, there is mixed evidence of correlated wind**

**speeds and direction from stereo-SCIDAR Shepherd et al. (2014), which might be worth including in our simulations.**

To realistically simulate atmospheric PSFs at Rubin Observatory or other wide-field instruments, we must account for the way the weather in the observatory environment influences correlations on the focal plane. This means it is important to use, as input to simulations, winds and turbulence profiles that have realistic correlations in altitude as well as realistic distributions over time. This is what we aim to do with PSF-WEATHER-STATION, the software package described in this paper.

In PSF-WEATHER-STATION, we use relevant sources of data about the telescope environment (both measurements and outputs of weather models) to produce input parameters for atmospheric PSF simulations. The package relies heavily on an empirical model of atmospheric turbulence proposed in Osborn et al. (2018) (hereafter OS18), which parameterizes relative turbulence strength at different altitudes in the atmosphere as a function of the wind shear at that location.

Whereas OS18 focuses mainly on the fast prediction of turbulence as a function of altitude for real-time adaptive optics corrections in ELT-class telescopes, our focus is a tool that can deliver atmospheric conditions which, in an ensemble sense, generate atmospheric PSFs that are representative of the site in question. We achieve this through the inclusion of site-specific telescope weather tower telemetry and historical MASS-DIMM distributions so that PSF-WEATHER-STATION can be used to predict and study the expected anisotropies in the PSF, the effect of various weather patterns, etc., at the location of a specific observatory.

In this paper we present the package as used for studies of the expected PSF at Rubin Observatory and Cerro Tololo Inter-American Observatory (CTIO) – the sites for the future Legacy Survey of Space and Time (LSST) and the current Dark Energy Survey (DES), respectively. However, the code is flexible enough to use for other observatories and includes functionality to download necessary datasets from weather forecasting services. Describe atmospheric system and how we simulate observations in Section 2, outline the PSF-WEATHER-STATION package in Section 3, and validate its use with DECam observations in Section 4.

## 2. IMAGING THROUGH A TURBULENT ATMOSPHERE

Since stars (and galaxies) are effectively light sources at infinity, their light can be treated as plane waves when entering the upper atmosphere. During the  $\sim 20$  km journey through the atmosphere, points on the surface of a wavefront (light entering the atmosphere with uniform phase) accrue relative phase shifts; the atmospheric component of an object’s PSF is the result of the spatial variations in the object’s wavefront phase across the telescope pupil. To quickly summarize the details, perturbations in air density in the atmosphere, driven by turbulent mixing of air at different temperatures, cause index of refraction perturbations  $\delta n$  (Lawrence & Strobel 1970; Clifford 1978) which we call *optical turbulence*. These fluctuations in  $n$  (referred to as *optical turbulence*) vary in space and time; therefore, each photon in general incurs a slightly different cumulative phase shift on its path to the telescope pupil. It is convenient to define an “atmospheric column”, with diameter roughly that of the telescope pupil, which delineates the volume of turbulent air sampled by the imaged photons from a single source. The atmospheric columns for each object in the field of view overlap at the pupil but diverge with distance from the telescope, resulting in a spatially varying, spatially correlated PSF over the focal plane.

Optical turbulence exists for a range of spatial scales and amplitudes. The spectral density of this turbulence, as a function of these spatial frequencies  $\kappa$ , can be described by the von Kármán power spectrum (von Kármán 1948; Tokovinin et al. 1998):

$$E_{\text{vK}}(\kappa) \propto (|\kappa|^2 + L_0^{-2})^{-11/6}. \quad (1)$$

This is a modification of Kolmogorov’s  $\kappa^{-11/3}$  power law (Kolmogorov 1941), imposing a finite upper bound on the physical scale of variations  $\delta n$  (i.e. lower bound on frequencies  $\kappa$ ) the scale of optical turbulence size of allowed turbulent variations via the (altitude dependent)

outer scale parameter  $L_0$ <sup>1</sup>. The von Kármán turbulence spectrum has an associated spatial correlation function (i.e., the Fourier transform of Equation 1). The degree of correlation for optical turbulence at a given altitude is set by the turbulence structure constant  $C_n^2$ ; as a function of altitude  $h$ , this is known as the optical turbulence profile (OTP)  $C_n^2(h)$ . Although turbulence is constantly evolving with time, OTPs are typically taken as constant during the course of an exposure.

Image quality is related to the OTP via the turbulence integral  $J$ :

$$J = \int_{h_1}^{h_2} C_n^2(h) dh. \quad (2)$$

When the integration bounds  $h_1, h_2$  correspond to the entire vertical extent of the atmosphere,  $J$  quantifies the total strength of the turbulence experienced by photons passing through the corresponding atmospheric column.  $C_n^2$  and  $J$  have units of  $\text{m}^{-2/3}$  and  $\text{m}^{1/3}$ , respectively. A related parameter which encodes similar information about image quality is the Fried parameter  $r_0$ . This characteristic length scale defines the radius of an aperture in which the wavefront phase variance is approximately  $1 \text{ rad}^2$  (Fried 1965). It depends on  $J$ , as well as zenith angle  $\zeta$  and wavenumber  $k$ :

$$r_0 = (2.914 k^2 \sec \zeta J)^{-3/5}. \quad (3)$$

Image quality, in terms of the PSF size, is approximately proportional to  $r_0^{-1}$ : in low turbulence conditions  $r_0$  is large (and  $J$  is small), and thus the PSF size is small (Roddier 1981).

The atmosphere is not a static system; as well as turbulent mixing, wind drives large scale motion of air. The components of wind velocity parallel to the telescope pupil are the relevant ones here, as **in a simplistic view** they translate the optical turbulence en masse across an atmospheric column. This temporal effect must be included in our understanding of the atmospheric system in the context of imaging, since the translation of optical turbulence during an exposure leads to correlated phase offsets for photons that are spatially separated at the pupil.

In order for atmospheric PSF simulations to be computationally tractable, the picture of atmospheric turbulence presented above must be simplified, as presented in the next section.

### 2.1. Atmospheric PSF simulations

<sup>1</sup> Not to be confused with the wavefront outer scale, the spatial scale at which correlations in wavefront phase vanish (Tokovinin et al. 1998; Borgnino 1990).

It is computationally intractable to simulate a PSF by calculating the trajectory of each photon through a turbulent (i.e., chaotic) 3D volume of atmosphere. Below, we briefly summarize an alternate method used to simulate atmospheric PSFs in the context of weak lensing surveys – see Jee & Tyson (2011); Peterson et al. (2015); ? for more details.

Measurements of optical turbulence with SCIntillation Detection And Ranging (SCIDAR) instruments show that the atmosphere is often stratified into regions of stronger turbulence separated in altitude by areas of relative calm (Osborn et al. 2018; Osborn & Sarazin 2018). Typically only  $\sim 1$  km in vertical extent, these *layers* of stronger turbulence dominate the atmospheric contribution to the PSF. These observations motivate a simplified model of the atmosphere that consists of only 2-dimensional *phase screens* across which the refractive index varies, with each screen representing one of these turbulent layers.

The refractive index variations within each phase screen are a realization of von Kármán turbulence. We assume Taylor’s frozen flow hypothesis (Taylor 1938), in which the time scales for changes in turbulence are longer than those for changes due to phase screen drift from wind. Under this assumption, it is not necessary to evolve the turbulence structure during a simulated exposure. Instead, each phase screen is assigned a “wind” speed and direction; for each time step  $\Delta t$  of the simulation, the phase screens are translated accordingly. After each wind update, the phase screen contributions within the atmospheric column (for each star in the field) are vertically summed. For each star, the sum is then Fourier transformed to focal plane coordinates and, after all time steps, added together to form the simulated image – i.e., the PSF. A cartoon of such an atmospheric simulation, with two phase screens, is depicted in Figure 1.

From this point, we will describe the details of atmospheric PSF simulations in terms of the GALSIM<sup>2</sup> (Rowe et al. 2015) implementation, but the principles hold for any workflow. To set up the simulation of a single-exposure PSF (in the call to `galsim.Atmosphere`), one must define the environmental and turbulence parameters discussed above. A building block of the simplified atmospheric model described above is the phase screen; one must define how many screens to include and, for each screen, set the following parameters: wind vector (speed and direction), altitude, outer scale, and turbulence integral contribution.

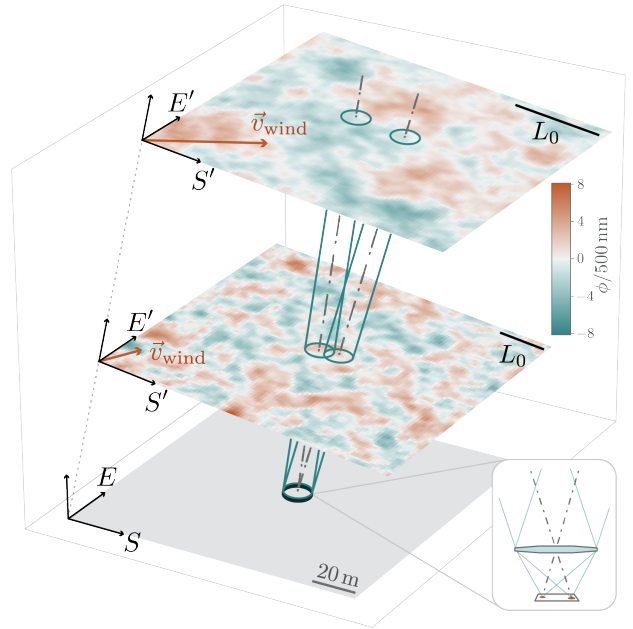


**Figure 1.** This schematic illustrates the simplified view of the atmosphere used for PSF simulations based on discrete phase screens. Lines of sight (dot-dashed grey) for two stars (whose images are located at extrema of the field of view) pass through two phase screens of von Kármán refractive index variations, each with different values for the outer scale  $L_0$ . The phase offset incurred by light passing through each point on each screen is indicated by the color scale in units of wavelength. The columns (teal) associated with each line of sight show the path of starlight that will reach the telescope aperture (black), along with the relevant phase screen area. The wind vectors (orange arrows) show speed and direction of the wind in the plane of the screen. The primed coordinate systems are perpendicular to the telescope axis, and are related to the ground coordinate system via the altitude and azimuth of the pointing.

Turbulence strength is described in GALSIM with the Fried parameter  $r_0$ , which determines the power spectrum amplitude for the total turbulence across all screens, and the relative weights  $w_i$ , which describe the contribution from each phase screen  $i$  to the total turbulence integral  $J$ . Turbulence integrals  $J$  add linearly, so contributions to  $r_0$  from each screen satisfy  $r_0 = (\sum_i w_i r_{0i}^{-5/3})^{-3/5}$ <sup>3</sup>. By convention, the value of  $r_0$  is specified for  $\lambda = 500$  nm and zenith angle  $\zeta = 0$ ; the wavelength and zenith dependence of  $r_0$  are used in GALSIM to calculate the value of  $r_0$  for other wavelengths and angles.

In this paper we adopt the meteorologic convention of defining wind direction; namely, wind direction de-

<sup>2</sup> <https://github.com/GalSim-developers/GalSim>

<sup>3</sup> The  $w_i$  parameter is denoted as  $r_{0\_weights}$  in GALSIM, but they are really weights to the turbulence integral  $J$ .

scribes the direction *from* which the wind is blowing. We define this angle in degrees East of North. Unless otherwise specified, we will use ground coordinates for all parameters (the unprimed system in Figure 1).

### 3. PSF-WEATHER-STATION OVERVIEW

A potential source of bias in weak lensing surveys is uncorrected, spatially correlated sources of noise. The atmosphere is correlated via the von Kármán power spectrum described in Equation 1 and, as we have seen, these spatial correlations translate into angular correlations in the size and shape of the atmospheric PSF in the associated exposure. Wind over the telescope plays an integral role in this process, as it moves correlated patches of turbulence through the atmospheric columns that impact the images of different objects, leading to correlations on larger angular scales. Although wind varies with altitude, if wind directions are consistent across altitudes, turbulence at all altitudes will move coherently, thereby imprinting a stronger correlation in the PSF than when wind directions at different altitudes are uncorrelated. Another relevant factor for PSF correlations is the altitude-dependence of the optical turbulence profile (OTP), which describes the contribution of each layer to the total turbulence strength. Interestingly, one of the drivers of atmospheric turbulence is wind itself – specifically, wind shear – so we expect that these two factors that influence spatial correlations in PSF parameters are not independent.

We separate the atmosphere into two regions based on the typical turbulence regime for those altitudes. The ground layer (GL) is typically defined to be from ground level to 500 – 1000 m above the telescope; in this region, complex topography and heat sources generate non-Kolmogorov eddies. The free atmosphere (FA) is the atmosphere above the ground layer; in this region, there are only a few sources of energy so turbulence is generally well-described by Kolmogorov statistics. This separation into GL and FA plays an important role in many design choices for PSF-WEATHER-STATION.

#### 3.1. Data inputs to PSF-WEATHER-STATION

The primary sources of data for PSF-WEATHER-STATION are outputs of global circulation models (GCM) developed for weather prediction; these are produced by organizations such as the European Centre for Medium-Range Weather Forecasts<sup>4</sup> (ECMWF) and the National Oceanic and Atmospheric Administration National Cen-

ters for Environmental Prediction<sup>5</sup> (NOAA NCEP). These models cover the entire globe on a grid of 0.25-0.5 deg resolution and output forecasts for dozens of environmental parameters at a number of different altitudes between 0 and ~80 km above sea level. Every 6 hours a forecast is initialized with the current global conditions (based on assimilated data). Each forecast predicts up to two weeks out from its initialization; the outputs available are the starting conditions and the hourly predictions for the following two weeks. In what follows, we have chosen the ECMWF ERA5 reanalysis dataset for its denser coverage in altitude – 137 levels – which is important for capturing vertical wind gradients in the atmosphere. In Appendix A we provide more details on the ECMWF and NOAA NCEP forecasts and our reasons for choosing the ECMWF data set.

These forecast models give us robust predictions of wind and temperature throughout the atmosphere as a function of time. The accuracy of the predictions is limited near the ground, however, where interactions of the atmosphere with the ground are not accurately captured since topographical features are not modeled at scales smaller than ~1 km. We overcome this limitation in PSF-WEATHER-STATION by using measurements from a weather tower on the telescope site in place of GCM data for the GL. Since weather tower data are typically recorded every few minutes, the sampling times of the telemetry information can be matched to the GCM outputs used for the FA. The weather tower measurements are optional input to PSF-WEATHER-STATION but highly recommended since the GL is of significant importance for the PSF, contributing between 40 and 60% of the turbulence at many observatories (Tokovinin & Travouillon 2005; Tokovinin et al. 2005, 2003).

#### 3.2. Optical turbulence in PSF-WEATHER-STATION

Existing mesoscale models are successful at simulating optical turbulence around observatories (Masciadri & Jabouille 2001; Masciadri et al. 2017); however, such models are computationally prohibitive when many realizations need to be simulated. Useful parameterizations of optical turbulence as a function of environmental quantities – such as temperature, pressure, wind, and kinetic energy – can be adapted from this literature, however, as is done in OS18. In particular, OS18 approximate wind shear as the sole contributor to the kinetic energy term (i.e. wind shear sources turbulent mixing of air) and replace the temperature and pressure profiles from mesoscale simulations with GCM data. In

<sup>4</sup> <https://www.ecmwf.int/en/forecasts/datasets/>

<sup>5</sup> <https://www.ncei.noaa.gov/products/weather-climate-models/global-forecast>



exchange for coarser resolution and more limited accuracy, the OS18 empirical model produces near-instant estimates of  $C_n^2(h)$  which, as shown in OS18, are broadly consistent with stereo-SCIDAR measurements at Cerro Paranal.

The OS18 model captures variation in turbulence strength with altitude, but not the absolute strength; it requires calibration for the total turbulence  $J$ . In addition, we found that the OS18 model significantly underpredicts turbulence in the GL – this is expected behaviour since turbulence there is sourced by multiple factors besides wind shear. PSF-WEATHER-STATION combines this OS18 optical turbulence model with complementary information from the literature to produce correlated turbulence parameters – one  $J$  for each phase screen –, as described below.

MASS-DIMM measurements of atmospheric turbulence at a variety of sites show that turbulence contributions from the FA and the GL are *independent* (Tokovinin & Travouillon 2005; Tokovinin et al. 2005; Chun et al. 2009). Motivated by this independence, the turbulence in GL and FA layers are treated separately in PSF-WEATHER-STATION. The relative turbulence within the FA layers is calculated with GCM data and OS18, and the total GL and FA integrals are drawn from log-normal distributions fit to published quantiles of measurements of  $J_{GL}$  and  $J_{FA}$ .

In Figure 2 we visualize the steps taken from raw GCM data to simulation-ready parameters in PSF-WEATHER-STATION, with Gemini-South as an example site. Our data sources are ground layer telemetry from the weather tower at Gemini-S, ECMWF ERA5 data<sup>6</sup>, and empirical MASS+DIMM turbulence PDFs fit to FA and GL data from (Tokovinin & Travouillon 2005). The top two rows of the figure show six months of site telemetry and GCM measurements – temporal matching of the datasets is only depicted for a randomly chosen timestamp shown in bold; however, each GCM altitude profile in purple has a single co-temporal ground layer datapoint in orange. Particularly noteworthy is the distinctly non-uniform distribution of wind directions, both at ground and across most altitudes – see histograms in the right column for data density.

The randomly chosen example, in bold, will serve to illustrate our process throughout this and the following sections. For instance, the OS18 output for this data is shown in purple lines in the bottom panel of Figure 2, pale is uncalibrated and dark is after applying the

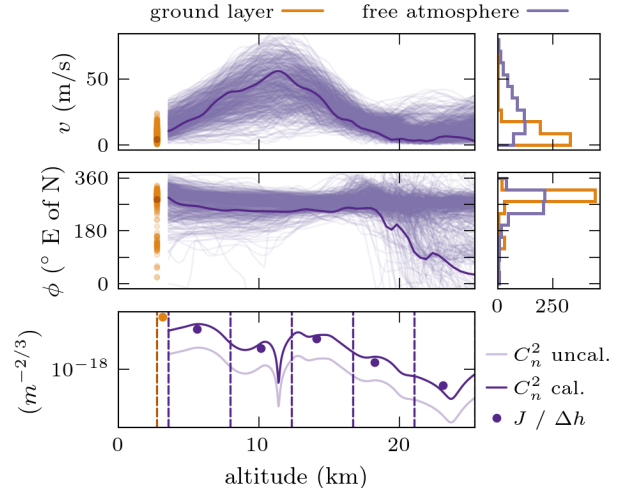


**Figure 2.** Six months of wind data at and above Cerro Pachón (05/01/2019 to 11/01/2019), processed with PSF-WEATHER-STATION as described in Section 3. We plot wind speed (top) and meteorological direction (direction of wind origin; middle) as a function of altitude, or as a frequency distribution on the right. Weather tower measurements of the ground layer (at an altitude of 50 m) are shown in orange; ECMWF ERA5 forecasts for the free atmosphere are shown in purple. The heavy purple line in each panel corresponds to data from the same random timestamp. In the bottom panel, the uncalibrated  $C_n^2(h)$  profile for this example time is shown in light purple; scaled by  $J_{FA}$ , the calibrated profile is in dark purple. The dashed vertical lines depict the boundaries between the altitude bins used to calculate turbulence integrals  $J$  for each FA phase screen. Each  $J$  is plotted scaled by the width of its corresponding altitude bin.

randomly chosen  $J_{FA}$  calibration. We choose to calculate turbulence integrals for  $N=6$  atmosphere layers; the PSF-WEATHER-STATION default is to create one layer for the ground, and divide the free atmosphere equally into  $N - 1$ . This is meant to allow flexibility in the number and altitude of turbulence layers, which as seen in SCIDAR data are not fixed in time (OS18). The boundaries between these 6 layers are shown in purple dashed vertical lines (the ground altitude is shown in orange dashed). Turbulence integrals are shown scaled by layer width for visualization, and placed at the default phase screen altitudes, i.e. the  $C_n^2$  center of mass within each FA layer and the middle of the GL. The set of parameters  $p_{psfws}$  returned by PSF-WEATHER-STATION is complete once we interpolate the wind speed  $v$  and direction  $\phi$  profiles to the phase screen altitudes  $h$ :  $p_{psfws} = \{J, h, v(h), \phi(h)\}$

Using random draws from turbulence distributions for ground turbulence integrals and calibration of FA  $C_n^2$  is not an optimal solution since these values aren't temporally correlated with other environment param-

<sup>6</sup> The closest grid point to Cerra Pachón, at -30.241, -70.737, is  $\sim 1.9$  km away at -30.25, -70.75.

ters. There is currently mixed observational evidence for whether a correlation exists between ground wind speed and  $J_{\text{GL}}$ , so while we include in PSF-WEATHER-STATION an option to correlate the random  $J_{\text{GL}}$  draws with ground wind speed it is by default correlation set to zero. There’s no evidence of correlation between  $J_{\text{FA}}$  and FA wind speeds – and the model already includes dependence on wind shear – so we have no analogous option in this regime. This method of using random draws from empirical distributions does somewhat restrict the predictive capabilities of simulations run with PSF-WEATHER-STATION, as we do not expect to recover the seeing on individual nights; however, we expect to recover overall seeing statistics as well as spatial correlations of the PSFs.

#### 4. VALIDATION

PSF-WEATHER-STATION uses multiple sources of telemetry and vetted models to generate sets of correlated parameters for PSF simulations. In this section, we describe validation tests of these generated parameters. These tests aim to answer the following: how simulations run with PSF-WEATHER-STATION parameters vary from the previous generation of atmospheric PSF simulations (Section 4.1), and how simulations run with PSF-WEATHER-STATION parameters compare to atmospheric PSFs as measured with a survey telescope (Section 4.3).

##### 4.1. Simulations at Cerro Pachón

The first validation study compared atmospheric PSF simulations for Rubin run with input parameters set in three different ways. In the first condition, parameters are generated for Cerro Pachón using PSF-WEATHER-STATION and the data summarized in Figure 2. The simulated PSF from one of these parameter sets (the example discussed in Section 3.2) is displayed in Figure 3; the spatial dependence of the PSF parameters across the field of view is clearly anisotropic.

As a benchmark we use the simulation parameters used in the DESC Data Challenge 2 (DC2) image simulations (The LSST Dark Energy Science Collaboration et al. 2021) as the second simulation condition. For each of  $N=6$  phase screens, wind speed and direction are drawn from uniform distributions between 0-20 m/s and 0-360°, respectively. Small Gaussian variations around the turbulence integrals from Ellerbroek (2002) are introduced, but the associated 6 altitudes remain fixed between simulations.

We label these first two conditions as *psfws* and *rand*. We wanted to identify whether the differences between these two conditions are mainly driven by the highly

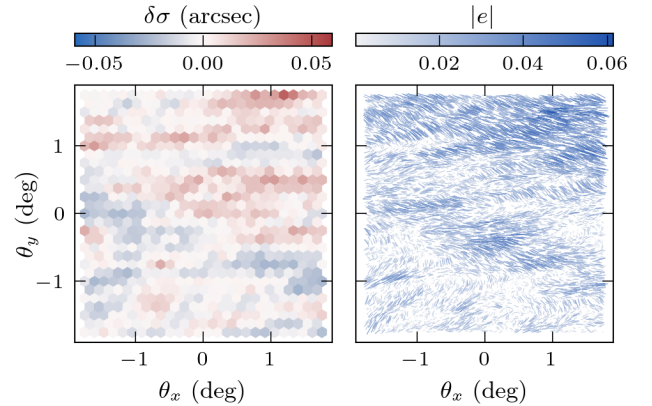


**Figure 3.** Left: map of PSF size variation, and right: whisker plot of ellipticity, on a  $3.5 \text{ deg}^2$  field. This PSF simulation was run with the PSF-WEATHER-STATION parameters in bold from Figure 2.

correlated wind directions in *psfws*. The third parameter condition was meant to address this question: *rand-Match* is identical to *rand* except we draw wind directions from PSF-WEATHER-STATION for the 6 fixed layers.

Simulations are run from the three conditions as follows: a set of three 30 s exposure is simulated, using each of the environmental conditions, from 150 different starting points, i.e., a set of phase screens with some given turbulence structure. Each triplet of simulations has the same outer scale (drawn from a truncated log normal with median of 25 m) and the same seeing (drawn uniformly from 0.6 to 1.6 arcsec); the fraction of this value contributed by each phase screen varies according to the turbulence integrals. To compare only the effect due to the difference in environmental parameters, the *psfws* simulations are also run with  $N = 6$  phase screens, but their altitudes are allowed to vary according to the  $C_n^2$  scheme described in Section 3.2.

##### 4.2. Simulation comparison results

We don’t expect anything from pairwise comparison of simulations, since we are interested in the comparison between the statistics of spatial correlations between the three sets of simulations. To run comparison, compute the anisotropic 2pcf map of each PSF parameter (size, shape). The average over the ensemble of simulations can tell us about dominant anisotropies – see Figure 4.

We also want to understand how the simulated PSF patterns relate to the input parameters for each simulation. To summarize the anisotropic 2pcf of each simulation, we extract a dominant direction: slice and max, see Figure 4 for example.

Results of correlating to input wind directions and speeds summarized in the nonexistent figures.

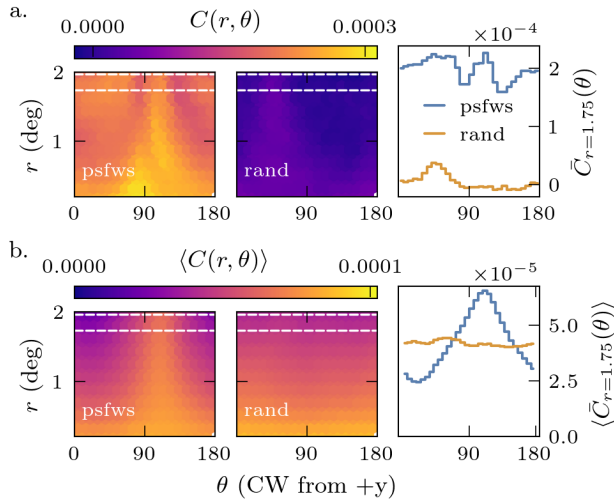


Figure 4.

#### 4.3. Data from Cerro Telolo

How do simulations run with psfws at Cerro Telolo compare to DES optics-removed data? coordinate swap between atm and GALSIM

#### 4.4. Data comparison results

### 5. CONCLUSION

- configuration details in github repo
- flexible model for simulation parameter generation – code to download and format additional GCM data from either ECMWF or NOAA is included with the package; can do this for any location and duration (starting from...?).
- (hopefully) reliably reproduces realistic correlations at CP

- 1 Morgan, Mike J for code review, PF, Sowmya, Sid for
- 2 discussions. J Osborn for sharing expertise. We ac-
- 3 knowledge ECMWF for access to the weather forecast
- 4 data through the MARS access system.
- 5 CSGF grant number, DARE funding
- 6 DESC blurb

## APPENDIX

### A. CHOICE OF GCM

Multiple efforts across the world generating high-quality weather forecasts. A few different considerations affect the choice of dataset to use:

1. Re-analysis vs forecast: many GCM models have "re-analysis" datasets available, which are past forecasts rerun with present-day state of the art numerical and data assimilation methods
2. For our particular use case, useful to have high vertical spatial resolution available (the model levels sample 137 point in altitude) which enables us to capture important wind gradients in the atmosphere.
3. horizontal spatial resolution: how far from observatory are you sampling
4. temporal sampling: how frequently do you get model outputs?

**make a table summarizing ECMWF and NOAA datasets?** The ERA5 data is available for each hour of the day and is sampled uniformly over the Earth's surface with 31km resolution.

These two considerations led us to use the ERA5 reanalysis catalog of the European Center for Medium-range Weather Forecasts (ECMWF)<sup>7</sup>, although for dates after February 2022, the NOAA GFS is also available with the same vertical resolution.

ECMWF is a non-hydrostatic model, more details in Osborn & Sarazin (2018) and...

## REFERENCES

<sup>7</sup> <https://www.ecmwf.int/en/forecasts/datasets/>

- Borgnino, J. 1990, *Applied Optics*, 29, 1863
- Chang, C., Marshall, P. J., Jernigan, J. G., et al. 2012, *Monthly Notices of the Royal Astronomical Society*, 427, 2572, doi: [10.1111/j.1365-2966.2012.22134.x](https://doi.org/10.1111/j.1365-2966.2012.22134.x)
- Chun, M., Wilson, R., Avila, R., et al. 2009, *Monthly Notices of the Royal Astronomical Society*, 394, 1121, doi: [10.1111/j.1365-2966.2008.14346.x](https://doi.org/10.1111/j.1365-2966.2008.14346.x)
- Clifford, S. F. 1978, in *Laser Beam Propagation in the Atmosphere*, ed. J. W. Strohbehn, Vol. 25 (Springer Berlin Heidelberg), 9–43, doi: [10.1007/3540088121\\_16](https://doi.org/10.1007/3540088121_16)
- Ellerbroek, B. L. 2002, *Journal of the Optical Society of America A*, 19, 1803, doi: [10.1364/JOSAA.19.001803](https://doi.org/10.1364/JOSAA.19.001803)
- Fried, D. L. 1965, *Journal of the Optical Society of America*, 55, 1427, doi: [10.1364/JOSA.55.001427](https://doi.org/10.1364/JOSA.55.001427)
- Heymans, C., Rowe, B., Hoekstra, H., et al. 2012, *Monthly Notices of the Royal Astronomical Society*, no, doi: [10.1111/j.1365-2966.2011.20312.x](https://doi.org/10.1111/j.1365-2966.2011.20312.x)
- Jarvis, M., Sheldon, E., Zuntz, J., et al. 2016, *Monthly Notices of the Royal Astronomical Society*, 460, 2245, doi: [10.1093/mnras/stw990](https://doi.org/10.1093/mnras/stw990)
- Jee, M. J., & Tyson, J. A. 2011, *Publications of the Astronomical Society of the Pacific*, 123, 596, doi: [10.1086/660137](https://doi.org/10.1086/660137)
- Kolmogorov, A. 1941, *Doklady Akademii Nauk S.S.S.R.*, 30, 301
- Lawrence, R., & Strohbehn, J. 1970, *Proceedings of the IEEE*, 58, 1523, doi: [10.1109/PROC.1970.7977](https://doi.org/10.1109/PROC.1970.7977)
- Masciadri, E., & Jabouille, P. 2001, *Astronomy & Astrophysics*, 376, 727, doi: [10.1051/0004-6361:20010999](https://doi.org/10.1051/0004-6361:20010999)
- Masciadri, E., Lascaux, F., Turchi, A., & Fini, L. 2017, *Monthly Notices of the Royal Astronomical Society*, 466, 520, doi: [10.1093/mnras/stw3111](https://doi.org/10.1093/mnras/stw3111)
- Osborn, J., & Sarazin, M. 2018, *Monthly Notices of the Royal Astronomical Society*, 480, 1278, doi: [10.1093/mnras/sty1898](https://doi.org/10.1093/mnras/sty1898)
- Osborn, J., Wilson, R. W., Sarazin, M., et al. 2018, *Monthly Notices of the Royal Astronomical Society*, 478, 825, doi: [10.1093/mnras/sty1070](https://doi.org/10.1093/mnras/sty1070)
- Peterson, J. R., Jernigan, J. G., Kahn, S. M., et al. 2015, *The Astrophysical Journal Supplement Series*, 218, 14, doi: [10.1088/0067-0049/218/1/14](https://doi.org/10.1088/0067-0049/218/1/14)
- Roddier, F. 1981, in *Progress in Optics*, Vol. 19 (Elsevier), 281–376, doi: [10.1016/S0079-6638\(08\)70204-X](https://doi.org/10.1016/S0079-6638(08)70204-X)
- Rowe, B., Jarvis, M., Mandelbaum, R., et al. 2015, arXiv:1407.7676 [astro-ph]. <http://arxiv.org/abs/1407.7676>
- Shepherd, H. W., Osborn, J., Wilson, R. W., et al. 2014, *Monthly Notices of the Royal Astronomical Society*, 437, 3568, doi: [10.1093/mnras/stt2150](https://doi.org/10.1093/mnras/stt2150)
- Taylor, G. I. 1938, *Proceedings of the Royal Society of London. Series A - Mathematical and Physical Sciences*, 164, 476, doi: [10.1098/rspa.1938.0032](https://doi.org/10.1098/rspa.1938.0032)
- The LSST Dark Energy Science Collaboration, Abolfathi, B., Alonso, D., et al. 2021, *The Astrophysical Journal Supplement Series*, 253, 31, doi: [10.3847/1538-4365/abd62c](https://doi.org/10.3847/1538-4365/abd62c)
- Tokovinin, A., Baumont, S., & Vasquez, J. 2003, *Monthly Notices of the Royal Astronomical Society*, 340, 52, doi: [10.1046/j.1365-8711.2003.06231.x](https://doi.org/10.1046/j.1365-8711.2003.06231.x)
- Tokovinin, A., & Travouillon, T. 2005, *Monthly Notices of the Royal Astronomical Society*, 365, 1235, doi: [10.1111/j.1365-2966.2005.09813.x](https://doi.org/10.1111/j.1365-2966.2005.09813.x)
- Tokovinin, A., Vernin, J., Ziad, A., & Chun, M. 2005, *Publications of the Astronomical Society of the Pacific*, 117, 395, doi: [10.1086/428930](https://doi.org/10.1086/428930)
- Tokovinin, A. A., Ziad, A., Martin, F., et al. 1998, *Kona, HI*, 1155, doi: [10.1117/12.321672](https://doi.org/10.1117/12.321672)
- von Kármán, T. 1948, *Proceedings of the National Academy of Sciences*, 34, 530, doi: [10.1073/pnas.34.11.530](https://doi.org/10.1073/pnas.34.11.530)